Nuclear Physics **A367** (1981) 237–268

MEASUREMENTS OF THE TOTAL PHOTONUCLEAR CROSS SECTIONS FROM 30 MeV TO 140 MeV FOR Sn, Ce, Ta, Pb AND U NUCLEI

A. LEPRÊTRE, H. BEIL, R. BERGÈRE, P. CARLOS, J. FAGOT, A. DE MINIAC and A. VEYSSIÈRE

Département de Physique Nucléaire, CEN Saclay, 91191 Gif-sur-Yvette Cedex, France

Received 12 December 1980
(Revised 14 April 1981)

Abstract: The total photonuclear absorption cross section for Sn, Ce, Ta, Pb and U has been studied from 25 to 140 MeV using a continuously variable monochromatic photon beam obtained from the annihilation in flight of monoenergetic positrons. The basic experimental results are a set of data giving sums of inclusive multiple photoneutron production cross sections of the form $\sigma^{(i)}(E_\gamma) = \sum_{i=j} \sigma(\gamma, in : E_\gamma)$ for neutron multiplicities ranging from $i = 1$ to 12. From these data the total photonuclear absorption cross section $\sigma(\text{tot} : E_\gamma)$ has been deduced. It is concluded that Levinger's modified quasideuteron model describes the total cross sections reasonably well. When these data are combined with lower energy data and integrated to 140 MeV they indicate the need for an enhancement factor K for the Thomas–Reiche–Kuhn sum rule of 0.76 ± 0.10. No evidence was found that would indicate an A-dependence for the enhancement factor.

E | PHOTONUCLEAR REACTIONS Sn, Ce, Ta, Pb, U(γ, xn), $E_\gamma = 25$–$140\downarrow$ MeV; measured $a(E_\gamma)$ summed for $x = 1$–12; deduced $\sigma(E_\gamma$, total), integrated σ, interaction models. Monochromatic photons.

1. Introduction

The measurement of the absolute value of the total photonuclear reaction cross section $\sigma(\text{tot} : E_\gamma)$ is particularly important in the photon energy range $30\,\text{MeV} < E_\gamma < 140\,\text{MeV}$, between the giant dipole resonance (GDR) and the pion photoproduction threshold. In this energy range the wavelength λ of the photon, which is absorbed by the nucleus, is much smaller than the dimensions of a heavy nucleus ($\lambda \simeq 2$ fm at $E_\gamma = 100$ MeV). One can thus hope to examine some nucleon–nucleon correlation effects which should show up for example, in the following experimental data.

The integrated cross section $\int^{140\,\text{MeV}} \sigma(\text{tot} : E_\gamma)\, dE_\gamma$. Such integrated cross sections systematically measured at Mainz [1]) for a set of light ($Z \leqslant 20$) nuclei, were found to be roughly twice the classical TRK energy-weighted sum rule $\sigma_0 = 0.06\, NZ/A$ MeV · b. To date there is no set of comparable data available for heavy nuclei. The first and main purpose of our experiments was therefore to complement

the Mainz data for heavy nuclei, throughout a range of A as large as possible. From such a set of systematic results, one can then hope to extract some information about the part of the residual nucleon–nucleon interaction, V_{NN}, which does not commute with the dipole (position) operator. In the various theoretical descriptions, this part of V_{NN} is referred to by different names, such as "velocity dependent term" or "exchange current contribution".

The energy dependence of $\sigma(\text{tot}: E_\gamma)$. If one can measure $\sigma(\text{tot}: E_\gamma)$ with good precision, the data should show a dependence upon E_γ which, in turn, might or might not show some connection with the cross section $\sigma_D(E_\gamma)$ for the photodisintegration of deuterium. Any resemblance (or lack of resemblance) between the shapes and the absolute values of $\sigma_D(E_\gamma)$ and $\sigma(\text{tot}: E_\gamma)$ might thus be connected to the classical quasi-deuteron (QD) model, introduced in 1951 by Levinger [2]), who predicted that the nuclear absorption of photons with wavelengths $\lambda \simeq 1$ to 2 fm should occur mostly on correlated neutron–proton pairs in the nucleus.

Finally, it will be shown that our method for measuring $\sigma(\text{tot}: E_\gamma)$ in heavy nuclei relies upon the measurement of all the partial photonuclear cross sections $\sigma(\gamma, in)$. Here $\sigma(\gamma, in)$ refers to all the decay channels for which, among the decay products, i neutrons are emitted. Such a method implies the simultaneous measurement of the *multiplicity* $\nu(E_\gamma)$ of the emitted neutrons and the evaluation of the average photoneutron multiplicity $\bar{\nu}(E_\gamma) = \sum_{i=1} i\sigma(\gamma, in)/\sigma(\text{tot}: E_\gamma)$. This $\bar{\nu}(E_\gamma)$ value depends upon the intranuclear cascade which follows the absorption of a photon in the nucleus and should therefore provide some information about final-state interactions, as well as decay mechanisms, in heavy nuclei.

Only the first two points will be examined in this paper. The decay properties will be described in another publication.

2. Experimental procedures

Before analyzing the various possible experimental procedures, it is worth summarizing the notation employed throughout this paper. $\sigma(\text{tot}: E_\gamma)$ is the total nuclear absorption cross section for photons of energy E_γ. $\sigma(\gamma, in: E_\gamma)$ or $\sigma(\gamma, in)$ is the sum of all the partial cross sections in which i neutrons are emitted, following the absorption of a photon of energy E_γ. For example the inclusive cross section $\sigma(\gamma, 3n)$ includes the decay channels $(\gamma, 3n)$, $(\gamma, 3np)$, $(\gamma, 3n\,2p)$, $(\gamma, 3n\alpha)$, etc. $\sigma(\gamma, xn) = \sum_{i=1}^{i_{MAX}} i\sigma(\gamma, in)$ is the neutron yield cross section (sometimes called the cross section for photoneutron production). $\sigma^{(j)}(E_\gamma) = \sum_{i=j}^{i_{MAX}} \sigma(\gamma, in: E_\gamma)$ is the sum of all the partial cross sections referring to the decay channels in which at least j neutrons are emitted following the absorption of a photon of energy E_γ.

Whereas a lot of studies of partial photoreaction channels in light nuclei were carried out before 1970, only very sparse data were obtained at that time for photoreactions on heavy nuclei with photons between 30 and 140 MeV. These rare measurements were always carried out by using continuous spectra of bremsstrah-

lung photons. The photonuclear absorption was identified either by detecting some of the emitted neutrons [3]) or through the study of the various radioactive residual nuclei [4,6]).

As an example of the first technique one must quote the 1953 experiment of Jones and Terwilliger [3]). They had two main difficulties to overcome in order to extract $\sigma(\text{tot}:E_\gamma)$ for heavy nuclei such as Ta, W, Pb, and U. First, they had to unfold bremsstrahlung yield data, in order to obtain a neutron yield cross section $\sigma(\gamma, x\text{n}) = \sum_i i\sigma(\gamma, i\text{n})$. The striking feature of their results was an appreciable rise in $\sigma(\gamma, x\text{n})$ between 40 and 140 MeV (a factor 1.6 for Ag increasing to about 4 for Pb and 5 for U). They also had to rely upon some empirical evaluation of the average multiplicity $\bar{\nu}(E_\gamma)$ of the neutrons emitted during the deexcitation process following the absorption of a photon E_γ by a nucleus. They thus found for Pb at $E_\gamma = 140$ MeV a very large value for $\sigma(\text{tot}:E_\gamma)$, namely

$$\frac{\sigma(\gamma, x\text{n})}{\bar{\nu}} = 30 \text{ mb} \simeq \sigma(\text{tot}:E_\gamma) ,$$

although they admitted a very large value for the neutron multiplicity, namely $\bar{\nu}(140 \text{ MeV}) = 9.3$. Neither of these large values for $\sigma(\text{tot}:140 \text{ MeV})$ and $\bar{\nu}(140 \text{ MeV})$ have been confirmed by later experiments. In the case of ^{181}Ta, they integrated their evaluated $\sigma(\text{tot}:E_\gamma)$ values up to 80 MeV and found $1.95\sigma_0$. An integration extended up to $E_\gamma \simeq 140$ MeV would then have led to a value significantly larger than $2\sigma_0$ for the integrated cross section. Once again these values should be considered as lower limits, due to the overestimation of $\bar{\nu}(E_\gamma)$ by Jones and Terwilliger.

As an example of the other technique, one can first refer to the 1967 experiment by Wyckoff, where a ^{209}Bi target was irradiated by a bremsstrahlung photon spectrum with an end point at 137 MeV. He could identify, through the final radioactive product nuclei, 8 $(\gamma, i\text{n})$ channels ($i = 2$ to 9) and 5 $(\gamma, 1\text{p}\, i\text{n})$ channels ($i = 4$ to 8). He could only give some model-dependent integrated cross-section data for each partial cross section, which could in turn be normalized to the integrated $\sigma(\gamma, 2\text{n})$ data, obtained in GDR measurements at other laboratories. When the Saclay GDR data [5]) are used for normalization purposes, the Wyckoff data lead to a lower limit of $\simeq 1.35\sigma_0$ for the total integrated cross section [4]) up to 137 MeV.

However, most of the systematic results obtained with this procedure came from the 1.5 GeV Lund electron synchrotron [6]). Yield curves were measured for several $^{197}\text{Au}(\gamma, k\text{n})^{197-k}\text{Au}^*$ and $^{127}\text{I}(\gamma, k\text{n})^{127-k}\text{I}^*$ interactions and energies between 75 and 800 MeV. The unfolding of these yield curves could then lead to the evaluation of the corresponding cross sections. By using the sum of these partial photoneutron cross sections, the Lund group could then give some lower limit values for the integrated total cross section $\int^{140 \text{ MeV}} \sigma(\text{tot}:E_\gamma)\, \text{d}E_\gamma$, namely,

$$3 \text{ MeV} \cdot \text{b} \simeq 1.06\sigma_0 \text{ for } ^{197}\text{Au} ,$$

$$3.1 \text{ MeV} \cdot \text{b} \simeq 1.67\sigma_0 \text{ for } ^{127}\text{I} .$$

Such a low value for ^{197}Au clearly shows that several important decay channels were not taken into account. Therefore any direct comparison of such a value with any modified sum rule (such as the Gell–Mann sum rule) is indeed very difficult. However an interesting feature appears in the sum of these partial photoneutron cross sections, which *decreases* slightly with energy from 50 MeV to the 120–140 MeV region, just as the cross section $\sigma_D(E_\gamma)$ for the photodisintegration of the deuteron does. This contradicts the previously cited Jones–Terwilliger results for Pb which showed an *increase* of $\sigma(\text{tot}: E_\gamma)$ from 18 mb to 30 mb when E_γ increases from 45 to 140 MeV.

One can surely consider these $\sigma(\text{tot}: E_\gamma)$, and their associated integrated cross-section experimental results for heavy nuclei, obtained with continuous bremsstrahlung spectra photons beams, as being only first approximations, to be refined later on as experimental techniques improved.

Clearly, better precision could be provided only by the use of "monochromatic" photon beams, especially when the actual number of "monochromatic photons" impinging upon the photonuclear target is counted for each measured $\sigma(\text{tot}: E_\gamma)$ point. Three methods, using such "monochromatic photon beams", have been developed since 1970 and are summarized below.

2.1. THE MAINZ METHOD

Here one measures the total photonuclear absorption cross section $\sigma(\text{tot}: E_\gamma)$ for each photon energy E_γ by measuring the total absorption cross section $\sigma_{\text{abs}}(E_\gamma)$ for $Z \leqslant 20$ nuclei and photon energies up to $E_\gamma \simeq 140$ MeV. The photon energy E_γ in the incident and emerging bremsstrahlung spectra are identified by means of two Compton spectrometers and one can thus write for any given E_γ:

$$\sigma(\text{tot}: E_\gamma) = \sigma_{\text{abs}}(E_\gamma) - \sigma_{\text{tot A}}(E_\gamma)\,,$$

where $\sigma_{\text{tot A}}(E_\gamma)$ is the total atomic absorption contribution from the classical photoelectric + Compton + pair production effects. To extract the required $\sigma(\text{tot}: E_\gamma)$ data one must compute a model-dependent value for $\sigma_{\text{tot A}}(E_\gamma)$. But, unfortunately, $\sigma_{\text{tot A}}(E_\gamma)$ varies as Z^2 and *increases* with E_γ from 30 to 140 MeV whereas $\sigma(\text{tot}: E_\gamma)$ varies only as Z and *decreases* with increasing E_γ. Some typical values for a set of nuclei and an intermediate photoenergy of $E_\gamma = 80$ MeV are given in table 1.

Moreover, such theoretical evaluations of $\sigma_{\text{tot A}}(E_\gamma)$ for medium and heavy nuclei, have rather large uncertainties $\Delta\sigma_{\text{tot A}}$ mostly due to the uncertain Coulomb correction term. For heavy nuclei such as Pb, the current uncertainties $\Delta\sigma_{\text{tot A}}$ are larger than the desired $\sigma(\text{tot}: E_\gamma)$ values, thus making any extension of this Mainz procedure to heavy nuclei highly problematic.

TABLE 1

Values of the total photonuclear cross section, $\sigma(\text{tot}: E_\gamma)$ and the total photoatomic cross section, $\sigma_{\text{tot A}}(E_\gamma)$ at $E_\gamma = 80$ MeV

	O	Ca	Sn	Pb
$\sigma(\text{tot}: E_\gamma)$ (mb)	1.5 [a])	3 [a])	8 [b])	14 [b])
$\sigma_{\text{tot A}}(E_\gamma)$ (mb) [c])	466	2380	12 800	30 800
$\frac{\sigma(\text{tot}: E_\gamma)}{\sigma_{\text{tot A}}(E_\gamma)}$	3.2×10^{-3}	1.3×10^{-3}	6×10^{-4}	4.5×10^{-4}
$\frac{\Delta\sigma_{\text{tot A}}}{\sigma_{\text{tot A}}}$ [d])	$<1\times10^{-3}$	$<210^{-3}$	$\sim5\times10^{-3}$	$\sim1\times10^{-2}$

[a]) Ref. [1]).
[b]) Present paper.
[c]) Ref. [21]).
[d]) The $\Delta\sigma_{\text{tot A}}$ errors were evaluated using data from ref. [8]).

2.2. THE BONN METHOD

At the 500 MeV Bonn synchrotron, monochromatic photons can be produced, in the energy range 215 MeV $< E_\gamma <$ 385 MeV, by tagging the photons of an incident bremmstrahlung spectrum. A group at Bonn recently undertook to detect the charged particles (p or π) emitted with $E_p > 60$ MeV or $E_\pi > 40$ MeV after the nuclear absorption of such a photon E_γ. Having thus measured a partial cross section, $\sigma(\gamma, \text{p or } \pi)$, one has to rely upon an intranuclear cascade model [9]) to ascertain the percentage r of the decay processes after absorption of a photon E_γ which leads to the emission of either a detectable proton ($E_p > 60$ MeV) or a pion ($E_\pi > 40$ MeV). The total photonuclear absorption is then assumed to be

$$\sigma(\text{tot}: E_\gamma) = \frac{\sigma(\gamma, \text{p or } \pi)}{r},$$

where r is close to 1 for light nuclei. However, $r \simeq 0.25$ at photon energies around $E_\gamma = 215$ MeV for Sn or Pb nuclei [10]).

Unfortunately, one should expect a still lower value of r for $E_\gamma < 140$ MeV, due to the closure of the π-channel and to an increased hindrance for proton emission by the Coulomb-barrier effect. For example, Chang and Wu [15]) computed, with their intranuclear cascade model, that following the absorption of a 100 MeV photon by a Pb nucleus: (a) 37% of the possible decay channels include at least 1 proton, and (b) 16% of the possible decay channels include at least a proton with $E_p > 10$ MeV. Only case (b) should be considered for a 1 mm thick Pb target, which would provide a very poor counting rate anyway (since no 4π proton detectors are yet easily available).

Thus the final total photonuclear cross section at $E_\gamma = 100$ MeV would be evaluated from a measurement of $\sigma(\gamma, \mathrm{p}: 100\ \mathrm{MeV})$ according to

$$\frac{\sigma(\gamma, \mathrm{p}: 100\ \mathrm{MeV})}{0.16} \simeq \sigma(\gamma, \mathrm{tot}: 100\ \mathrm{MeV}),$$

where the normalization factor $1/0.16 \simeq 6$ could only be known with the uncertainties inherent in such a model.

2.3. THE SACLAY METHOD

The Saclay group decided to extend the method used for measuring $\sigma(\mathrm{tot}: E_\gamma)$ of heavy nuclei in the GDR region, systematically used at Livermore and the 60 MeV Saclay linac [11]), to photon energies $E_\gamma > 30$ MeV. To do this two new experimental procedures had to be developed.

(i) One had to improve the "quality" of the existing Saclay variable energy quasi-monochromatic photon beam, obtained by the in-flight annihilation of monoenergetic positrons. Since a detailed description of this new Saclay facility has recently been published [12]), we shall merely recall the essential points. One shows that, for a certain loss in "monochromatic" photon beam intensity, the annihilation to bremsstrahlung ratio at a given photon-energy E_γ increases considerably with the observation angle, θ, with which the radiator is observed. The large monoenergetic positron currents (10 to 50 nA) produced by the ALS at energies between 20 and 145 MeV, thus allowed us to use only photons emitted around $\theta \simeq 4°$ and still to obtain roughly 10^4 monochromatic annihilation photons per second at the photonuclear target site.

(ii) One also had to improve the performance of a 4π, 250 litre, gadolinium-loaded liquid scintillator photoneutron detector, also previously described in the literature [13]). Such a detector has an efficiency of roughly $\varepsilon \simeq 65\%$ and, when observing a $(\gamma, i\mathrm{n}\, k\mathrm{p})$ event say, the ensuing, simultaneously emitted, i neutrons are first thermalized and dispersed in time before being absorbed and detected, in a time gate of $\simeq 25$ μs, by means of a (n, γ) capture in Gd. In principle, at least, such a facility allows for separate and simultaneous measurements of the partial photoneutron cross sections $\sigma(\gamma, i\mathrm{n})$ as a function of the photon energy E_γ. A detailed description of this experimental procedure for photoneutron multiplicities below 4 ($i < 4$), can be found in ref. [13]). Of course, in order to extend the measurements up to $E_\gamma \sim 140$ MeV, with the associated large multiplicities (which were measured up to $i = 12$), some important improvements had to be achieved. These were (a) to improve the mechanical and electronic shielding against beam-independent B_0 and beam-dependent B_b backgrounds, (b) to decrease the dependence of the detector efficiency upon the neutron energy, (c) to refine the mathematical processes by which the raw detector data are linked to the final desired $\sigma(\gamma, i\mathrm{n})$ values. The details of such improvements are described in a separate paper [14]). But even so, some

model-dependent errors (hopefully minor) still remain when evaluating $\sigma(\text{tot}:E_\gamma)$ where the latter can be expressed as:

$$\sigma(\text{tot}:E_\gamma) \simeq \sum_{i=1} \sigma(\gamma, i\text{n}) = \sigma^{(1)}(E_\gamma) .$$

Clearly, the above expression for $\sigma(\text{tot}:E_\gamma)$ does not include the partial cross sections in which *only* charged particles or photons are emitted. One can get a quantitative idea of the smallness of such an omission by using an intranuclear cascade model. For instance, Chang and Wu computed that, following the absorption of a 100 MeV photon by a Pb nucleus, less than 10^{-3} of $\sigma(\text{tot}:100\,\text{MeV})$ corresponds to decay channels containing charged particles only [15]). Their model predicts that the emitted protons should appear mostly in the $(\gamma, 1\text{p}\, i\text{n})$ channels, which are, in fact, included in our $\sigma(\gamma, i\text{n})$. A similar trend is displayed by experimental results. For example Shoda's measurements for ^{142}Nd and for ^{181}Ta showed that [16,17])

$$\int^{26\,\text{MeV}} \sigma(\gamma, \text{p})\, dE_\gamma \leqslant 3 \times 10^{-2} \int^{26\,\text{MeV}} \sigma(\gamma, \text{n})\, dE_\gamma .$$

No similar precise measurements exist for the higher energy range. However, some information can certainly be extracted from the recent study of the ^{209}Bi $(\pi^-, i\text{nyp})$ reaction, carried out at SIN with stopped pions which are captured by a quasideuteron, thus bringing into the nucleus an energy of ~140 MeV and no momentum (a situation somewhat similar to that expected for the absorption of a 140 MeV photon by a nucleus). It was found [18]) that the average neutron multiplicity was 6.8 ± 0.4 while the average proton multiplicity was only 0.37 ± 0.16.

One can therefore expect that, in a heavy nucleus such as lead, the omission of the $\sigma(\gamma, \text{p}) + \sigma(\gamma, 2\text{p}) + \sigma(\gamma, \alpha) + \cdots$ cross sections can only cause errors of roughly $\Delta\sigma(\text{tot}:E_\gamma) < 5 \times 10^{-2} \sigma(\text{tot}:E_\gamma)$. As will be seen later, such an error is smaller than the overall error bars pertaining to our measurements.

3. The evaluation of the $\sigma^{(j)}(E_\gamma)$ data and the experimental uncertainties

As pointed out before, the evaluation of $\sigma(\text{tot}:E_\gamma) \simeq \sum_{i=1} \sigma(\gamma, i\text{n})$ seems to imply the separate determination of the true partial cross sections $\sigma(\gamma, i\text{n}) \pm \Delta\sigma(\gamma, i\text{n})$ for each neutron multiplicity i. Actually we found it better to consider quantities defined by:

$$\sigma^{(j)}(E_\gamma) = \sum_{i=j} \sigma(\gamma, i\text{n}:E_\gamma) .$$

The reason for such a choice is that any of the above quantities $\sigma^{(j)}(E_\gamma)$ can be obtained with an uncertainty $\Delta\sigma^{(j)}$ much smaller than any of the uncertainties $\Delta\sigma(\gamma, i\text{n})$. Actually, when one computes $\Delta\sigma^{(j)}$, it turns out that one obtains [14]) a partial cancellation of the various $\Delta\sigma(\gamma, i\text{n})$ uncertainties. While the uncertainties

$\Delta\sigma(\gamma, in)$ are so large that the extraction of meaningful $\sigma(\gamma, in)$ data becomes very difficult, the uncertainties for the $\sigma^{(j)}$ results remain reasonable.

Any of the above cross sections $\sigma^{(j)}$, is obtained in a two-step measurement:

(a) During a typical two-hour run a given number, $Q = 0.8$ to 1.5×10^{15}, of monoenergetic positrons with a total energy E_+ passes through a low-Z radiator (LiH). Bremsstrahlung photons, which are continuous in energy, and annihilation photons with energy $E_\gamma = f(E_+, \theta)$, are emitted near the selected angle θ and impinge upon the photonuclear target. The energy spectrum $\phi_{LiH}(\omega)$ of these photons is represented in fig. 1A.

(b) Then, in the second step, the same number Q of monoenergetic positrons with the same energy E_+ passes through a high-Z radiator (Cu) of the same thickness in radiation lengths. For the same collimation around the angle θ, the photons represented by the spectrum $\phi_{Cu}(\omega)$ of fig. 1B will then impinge upon the same photonuclear target. During these two experiments the quantities actually measured are the yields Y_j(LiH) and Y_j(Cu). These are the number of events in which j neutrons are detected from the photonuclear target. Within the restrictions that corrections have been applied for all background contributions to the yields measured with the two radiators and that the counting rates are so low that pile-up

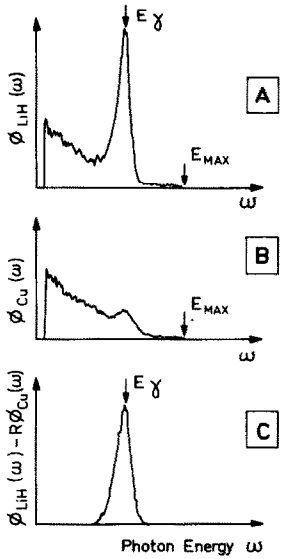

Fig. 1. (A) Typical photon spectrum $\phi_{LiH}(\omega)$, radiated at $\theta = 4°$ by $E_+ = 110$ MeV positrons passing through a LiH radiator, measured with a $8'' \times 12''$ NaI crystal. (B) Typical photon spectrum $\phi_{Cu}(\omega)$, radiated at $\theta = 4°$ by $E_+ = 110$ MeV positrons passing through a Cu radiator, measured with the same 20.3×30.5 cm NaI crystal. (C) Typical photon-difference spectrum $\phi_{LiH}(\omega) - R\phi_{Cu}(\omega)$ with the "monochromatic annihilation line" centered at $E_\gamma = 72$ MeV. The FWHM of this line is essentially determined by the 20.3×30.5 cm NaI resolution [12]) and the actual E_γ line width is much smaller than the one shown. The total number of "monochromatic annihilation photons" S, discussed in the text, is given by the area under the peak of (C).

effects can be neglected, these yields Y_j(LiH) [or Y_j(Cu)] are related to the number of photonuclear events, N_i(LiH) [or N_i(Cu)], of multiplicity i photoneutrons by the expression

$$Y_j = \sum_{i=j}^{m} W_{ij} N_i ,$$

where $j \leqslant i$ and m is the maximum neutron multiplicity possible due to the absorption by the target of a photon of energy $E_\gamma = E_{\max}$ and N_i and W_{ij} are given by:

$$N_i(\mathrm{LiH}) = \int_0^{E_{\max}} \phi_{\mathrm{LiH}}(\omega)\sigma(\gamma, i\mathrm{n}: \omega)\, \mathrm{d}\omega ,$$

$$N_i(\mathrm{Cu}) = \int_0^{E_{\max}} \phi_{\mathrm{Cu}}(\omega)\sigma(\gamma, i\mathrm{n}: \omega)\, \mathrm{d}\omega ,$$

$$W_{ij} = \frac{i!}{(i-j)!\, j!}\, \varepsilon^j (1-\varepsilon)^{i-j} .$$

Here ε is the efficiency of the neutron detector for detecting a single neutron. The total number of multiple neutron events detected, for example in the first experiment with the LiH radiator, can thus be written in the form:

$$Y^{(1)}(\mathrm{LiH}) = \sum_{j=1}^{m} Y_j(\mathrm{LiH}) .$$

Note that for $\varepsilon \to 0$, $Y^{(1)} \to Y_1 = \varepsilon(N_1 + 2N_2 + 3N_3 + \cdots + mN_m)$, i.e. it is proportional to an integral over the total neutron yield cross section. For $\varepsilon \to 1$, $Y^{(1)} \to N_1 + N_2 + N_3 + \cdots N_m$ and is proportional to an integral over the sum of all cross sections in which one or more neutrons are emitted.

The basic mathematical techniques connected with solving the m equations for Y_j to obtain the quantities N_i (i.e. a *neutron multiplicity* unfolding procedure), are akin to those associated with the analysis of bremsstrahlung yield curves to obtain photonuclear cross sections in the well-known *photon energy* spectrum unfolding procedure. A difference is that in the neutron multiplicity unfolding, the number m is much smaller than in the bremsstrahlung yield curve analysis and the efficiency matrix is better known than the bremsstrahlung matrix associated with the beam produced by a particular electron accelerator. Just as in the case of the analysis of bremmsstrahlung yield curves, where it was always possible to know the integral of the cross section to some upper energy limit E_m with a much smaller uncertainty than the average cross section over some energy bin at an energy $E_\gamma \leqslant E_m$, so in this case the quantities $N^{(j)} = \sum_{i=j}^{m} N_i$ can be determined with much smaller uncertainties than those associated with any single term N_k in $N^{(j)}$. It can be readily shown [14]) that N_k and $N^{(j)}$ and their uncertainties are given by matrix equations of the form; e.g.

$$N_k = \sum_i a_{ki} Y_i , \quad N^{(j)} = \sum_i b_{ji} Y_i .$$

As has been indicated above, the quantities N_i(LiH) [or N_i(Cu)] are integrals of the inclusive photoneutron cross section for the production of i neutrons over the spectra of photons represented in fig. 1A (LiH) or 1B (Cu). If the bremsstrahlung spectrum produced by positrons passing through a LiH radiator has the same shape as that when they pass through a Cu radiator and if, as is indicated by fig. 1C, it is possible to normalize these two spectra with a simple factor R to produce a spectrum that consists only of an annihilation peak at E_γ, then the summed cross section $\sigma^{(i)}(E_\gamma)$ is given by:

$$\sigma^{(i)}(E_\gamma) = \frac{N^{(i)}_{\mathrm{LiH}} - RN^{(i)}_{\mathrm{Cu}}}{S} \frac{A}{t\mathcal{N}},$$

where S is the total number of monochromatic photons with energy E_γ, shown in fig. 1C, namely

$$S = \int_0^{E_{\max}} [\phi_{\mathrm{LiH}}(\omega) - R\phi_{\mathrm{Cu}}(\omega)]\, \mathrm{d}\omega .$$

In this expression A is the mass number of the target nucleus, t is the target thickness in g/cm^2 and $\mathcal{N}$ is Avogadro's number. Typical figures are $S = 0.5$ to 1×10^8 and $t\mathcal{N}/A \simeq 6 \times 10^{21}$ atoms/cm^2. It should be emphasized here that the normalization factor R must be measured carefully for each experiment.

As an example of the order of magnitude of the figures involved one obtains, for a measurement of a Pb target (6.5×10^{21} atoms/cm^2) with $E_\gamma = 72$ MeV annihilation photons produced at $\theta \sim 4°$ by 110 MeV positrons:

$$\sigma^{(5)}(72\ \mathrm{MeV}) = \frac{N^{(5)}_{\mathrm{LiH}} - RN^{(5)}_{\mathrm{Cu}}}{S} \frac{A}{t\mathcal{N}} = \frac{6231 - 2569}{6.7 \times 10^7} \frac{A}{t\mathcal{N}} = 8.2 \pm 1.5\ \mathrm{mb},$$

$$\sigma^{(2)}(72\ \mathrm{MeV}) = \frac{N^{(2)}_{\mathrm{LiH}} - RN^{(2)}_{\mathrm{Cu}}}{S} \frac{A}{t\mathcal{N}} = \frac{30712 - 23981}{6.7 \times 10^7} \frac{A}{t\mathcal{N}} = 15.1 \pm 1.2\ \mathrm{mb},$$

where overall uncertainties of $\Delta\sigma^{(5)}/\sigma^{(5)} \simeq 0.20$ and $\Delta\sigma^{(2)}/\sigma^{(2)} \simeq 0.08$ are associated with the above values.

The three main error sources contributing to these uncertainties are:

(a) The statistical uncertainties, which are the predominant ones for our experimental conditions.

(b) The "subtraction errors", which should be associated with a possible error, $\Delta R/R \sim 2 \times 10^{-2}$, in our evaluation of the normalizing factor R between the LiH and the Cu bremsstrahlung spectra. This effect has been analyzed in detail in a previous paper [12]).

(c) The overall uncertainty $\Delta\varepsilon$ in the "actual" efficiency ε of the neutron detector. It consists of two parts, $\Delta\varepsilon'$ and $\Delta\varepsilon''$. First, an uncertainty, $\Delta\varepsilon'/\varepsilon \simeq 1 \times 10^{-2}$ is associated with the preliminary "off-line" measurement of $\varepsilon = \varepsilon_0$ using ^{252}Cf fission neutrons whose average energy is ~2.17 MeV. Second, in the formula used to

evaluate the quantities $N^{(j)}$ and finally $\sigma^{(j)}(E_\gamma)$, the coefficients $b_{ji}(\varepsilon)$ were computed numerically by making $\varepsilon = \text{constant} = \varepsilon_0$. Of course, the actual detection efficiency, $\varepsilon = f(E_n)$, depends upon the energy, E_n, of each particular photoneutron. But the energy E_n of a particular photoneutron, emitted in a (γ, in) reaction, is a function of the absorbed photon energy E_γ and the neutron multiplicity i. In such a photonuclear event one has to consider the average neutron energy, $\bar{E}_n$, and the associated "average" detection efficiency $\bar{\varepsilon} = f(\bar{E}_n)$.

Actually, both theoretical cascade models [15]) and a first analysis of our experimental data [19]) show that, following the absorption of a photon E_γ by a heavy nucleus, a fraction fE_γ of the excitation energy is carried off by the emission of n_f fast neutrons and (or) p_f fast protons, whereas the fraction $(1-f)E_\gamma$ excites a compound-nucleus final stage from which n_s slow neutrons are evaporated. These n_s maxwellian evaporation neutrons are emitted with an average kinetic energy $\simeq 2$ MeV and are actually detected with the efficiency ε_0. The actual neutron detector efficiency, $\varepsilon = f(E_n)$, published in a previous paper [13]), used Monte Carlo computations applied to a bare detector sphere filled with liquid scintillator. But in our experiment, the thick shielding surrounding this sphere reflects some of the escaping neutrons back towards the detector, which renders the decrease of ε with E_n much less important [14]) so that one still has $\varepsilon = 0.8\varepsilon_0$ for $E_n \geqslant 14$ MeV. Since, in the case of Pb [ref. [19])], one has an average value of $(\bar{n}_f/\bar{n}_s) < 20\%$, one can show that the $\varepsilon = C^t = \varepsilon_0$ assumption introduces a possible systematic error of $\Delta\varepsilon''/\varepsilon \leqslant 3\times 10^{-2}$. The overall possible error $\Delta\varepsilon/\varepsilon$, used for the computation of the $\Delta\sigma^{(j)}$ uncertainties, was thus assumed to be $\Delta\varepsilon/\varepsilon \simeq 3\times 10^{-2}$.

4. The $\sigma^{(j)}(E_\gamma)$ results

For reasons detailed in sect. 5, the overall statistical and systematic uncertainty $\Delta\sigma^{(1)}$, pertaining to $\sigma^{(1)}$, is much greater than the corresponding uncertainty $\Delta\sigma^{(2)}$ associated with $\sigma^{(2)}$. But we know that $\sigma^{(1)} \simeq \sigma^{(2)} + \sigma(\gamma, n) + \sigma(\gamma, pn)$, and hence the following question arises: can one assume, or demonstrate, that $\sigma^{(1)} - \sigma^{(2)} \simeq \sigma(\gamma, n) + \sigma(\gamma, pn)$ is small enough to be neglected for incident photons in the $30\ \text{MeV} \leqslant E_\gamma \leqslant 140\ \text{MeV}$ range?

If one can indeed neglect $\sigma^{(1)} - \sigma^{(2)}$ then most of the relevant information required for the evaluation of $\sigma(\text{tot}: E_\gamma)$ would be contained in $\sigma^{(2)}(E_\gamma)$ which has an appreciably smaller uncertainty $\Delta\sigma^{(2)}$ than the corresponding $\Delta\sigma^{(1)}$.

Turning again to the Chang and Wu model [15]), we note that they predict for ^{208}Pb

$$\sigma^{(1)} - \sigma^{(2)} \simeq 0.035\sigma(\text{tot}: E_\gamma) \text{ for } E_\gamma = 40\ \text{MeV},$$

$$\sigma^{(1)} - \sigma^{(2)} \simeq 0.011\sigma(\text{tot}: E_\gamma) \text{ for } E_\gamma = 70\ \text{MeV},$$

$$\sigma^{(1)} - \sigma^{(2)} \simeq 0.04\sigma(\text{tot}: E_\gamma) \text{ for } E_\gamma = 100\ \text{MeV}.$$

Very similar results were obtained with the Oak Ridge evaporation code PICA for the case of another heavy nucleus, ^{197}Au, by Pringle *et al.* [20]).

Assuming, therefore, (see also sect. 5) that our basic hypothesis,

$$\sigma(\text{tot}:E_\gamma) \simeq \sigma^{(2)}(E_\gamma)\,,$$

is reasonable, which means that it includes a systematic error $\sigma^{(1)} - \sigma^{(2)}$ which is smaller than the final experimental errors, we shall limit the presentation of our experimental data to $\sigma^{(j)}$ with $j \geq 2$ for the following nuclei: Sn, Ce, Ta, Pb and U.

4.1. THE Pb DATA

A first set of $\sigma^{(2)}(E_\gamma)$ results, for photon energies below $E_\gamma = 106$ MeV, has already been published [22]). In fig. 2 we present our $\sigma^{(j)}(E_\gamma)$ data for a 2.27 g · cm^{-2} thick natural Pb target and photon energies between 20 and 140 MeV. Arrows indicate the theoretical [21]) binding energies B_{jn}, of j neutrons in ^{208}Pb for $j \geq 3$. One observes very good agreement between the experimental onset of $\sigma^{(j)}(E_\gamma)$ and the corresponding threshold value B_{jn}, even though no threshold constraints whatsoever were imposed in computing $\sigma^{(j)}(E_\gamma)$ from the raw data. The continuous lines represent "smoothed average $\sigma^{(j)}(E_\gamma)$ plots", drawn through the error-bar weighted experimental points, which are expected to give the energy dependence of $\sigma^{(j)}(E_\gamma)$ more precisely since no structure is expected in the cross section in this energy range. One further notes that the relative uncertainties $\Delta\sigma^{(j)}/\sigma^{(j)}$ decrease with decreasing j, as previously indicated in the numerical example given for Pb at $E_\gamma = 72$ MeV.

The essential information contained in fig. 2 is summarized in fig. 3, where:

(i) $\sigma^{(2)}(E_\gamma)$ is assumed to be a reasonable representation of $\sigma(\text{tot}:E_\gamma)$, a point which will be more closely examined later on.

(ii) Individual $\sigma^{(j)}(E_\gamma)$ points and their experimental uncertainties are only given for the extreme j-values, namely $\sigma^{(2)}$ and $\sigma^{(10)}$ in this case.

(iii) The dashed as well as the full curves representing $\sigma^{(j)}(E_\gamma)$ for $j \geq 2$, are meant to give the "smoothed averages" drawn through the error bar weighted experimental points. Since no "structure" is expected in the photon energy interval shown, the uncertainties attached to these "averaged $\sigma^{(j)}(E_\gamma)$ plots" are surely smaller than the ones attached to the individual $\sigma^{(j)}(E_\gamma)$ points.

The following important point should also be mentioned here. Although the differences between any two consecutive smoothed curves in fig. 3, namely $\sigma^{(j)}(E_\gamma) - \sigma^{(j+1)}(E_\gamma)$, should indeed represent the so-called partial photoneutron cross section $\sigma(\gamma, jn:E_\gamma)$, the actual experimental uncertainties are such that one can merely consider such a difference as a very rough approximation to the true $\sigma(\gamma, jn:E_\gamma)$ photoneutron cross section.

4.2. THE Sn, Ce AND Ta DATA

The Sn, Ce and Ta experimental results, obtained with natural targets of 2.74, 5.7 and 2.7 g · cm^{-2} respectively, are shown in figs. 4 to 6. No individual $\sigma^{(j)}(E_\gamma)$ plots

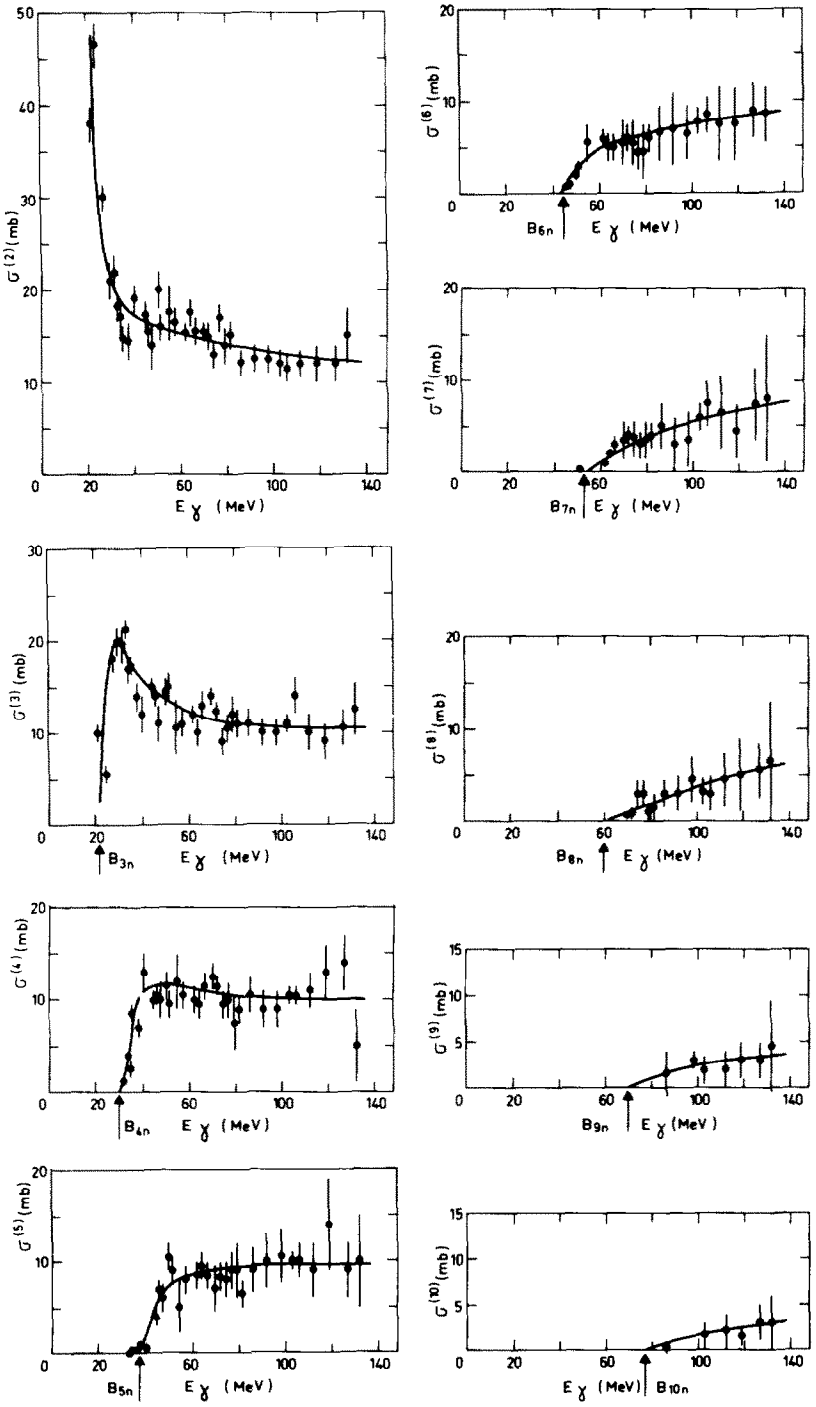

Fig. 2. Experimental $\sigma^{(j)}(E_\gamma)$ data points for Pb and photon energies between $E_\gamma = 20$ and 140 MeV are shown for $j = 2$ to 10. Arrows indicate theoretical [21]) neutron thresholds B_{jn} for the emission of $j \geq 3$ neutrons from ^{208}Pb. The full lines represent "smoothed average $\sigma^{(j)}(E_\gamma)$ plots" drawn through the error bar weighted experimental points (see text for details).

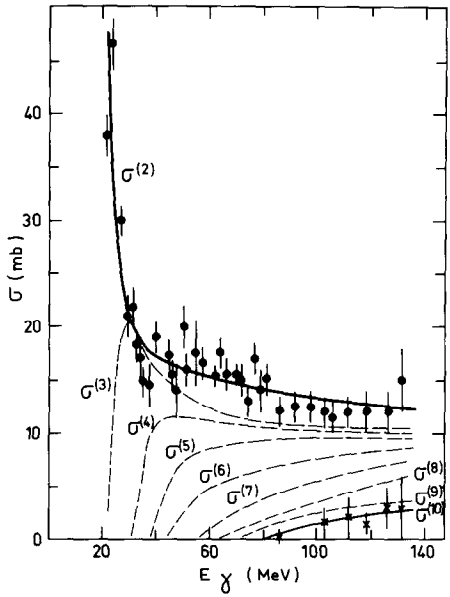

Fig. 3. Experimental $\sigma^{(2)}(E_\gamma)$ and $\sigma^{(\max)}(E_\gamma) = \sigma^{(10)}(E_\gamma)$ results for Pb and photon energies E_γ between 20 and 140 MeV. The solid and dashed lines represent "smoothed average $\sigma^{(i)}(E_\gamma)$ plots" drawn through the error-bar weighted experimental points. No data points are shown for intermediate $\sigma^{(i)}(E_\gamma)$ results which are only represented by the dashed curves.

will be shown and only a set of $\sigma^{(i)}(E_\gamma)$ curves, similar to those given in fig. 3 for Pb, will be presented for each of these nuclei. In figs. 4 to 6 only the $\sigma^{(2)}(E_\gamma)$ and $\sigma^{(\max)}(E_\gamma)$ data are shown as experimental results with their uncertainties and $\sigma^{(\max)}(E_\gamma)$ equals $\sigma^{(7)}$, $\sigma^{(8)}$ and $\sigma^{(9)}$ for Sn (fig. 4), Ce (fig. 5) and Ta (fig. 6),

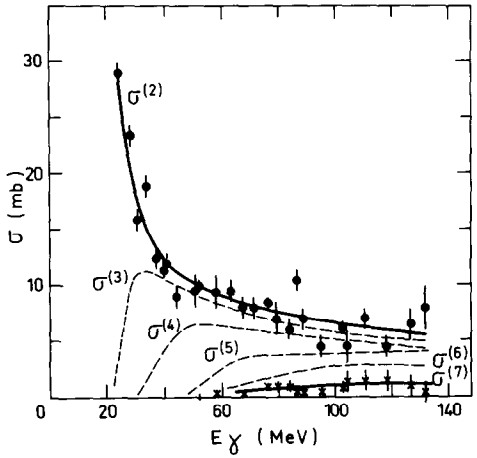

Fig. 4. Experimental $\sigma^{(2)}(E_\gamma)$ and $\sigma^{(\max)}(E_\gamma) = \sigma^{(7)}(E_\gamma)$ results for Sn. Remainder of caption as in fig. 3.

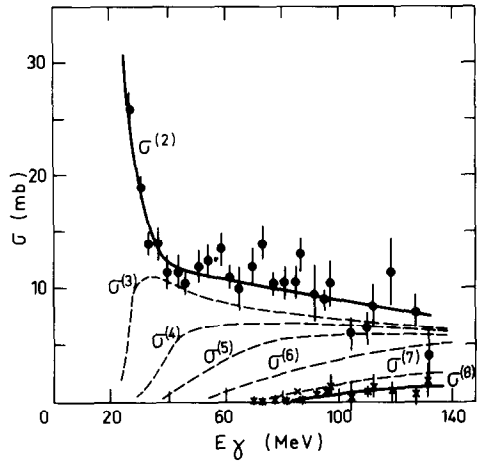

Fig. 5. Experimental $\sigma^{(2)}(E_\gamma)$ and $\sigma^{(\max)}(E_\gamma) = \sigma^{(8)}(E_\gamma)$ results for Ce. Remainder of caption as in fig. 3.

respectively. Intermediate $\sigma^{(j)}(E_\gamma)$ plots are indicated by dashed lines which represent smoothed averages drawn through the error bar weighted experimental points.

As for the plots of $\sigma^{(j)}(E_\gamma)$ with the largest (j) values, shown in figs. 2 to 6, their meaning can best be understood by means of an example. Let us consider the Ce case at $E_\gamma \simeq 134$ MeV shown in fig. 5. At such a photon energy, we might still have

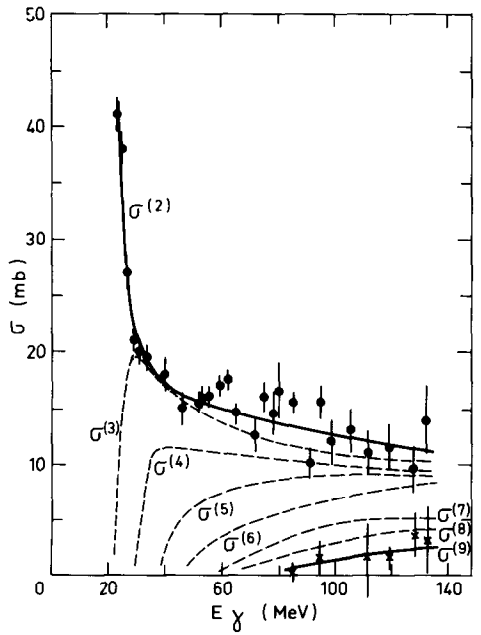

Fig. 6. Experimental $\sigma^{(2)}(E_\gamma)$ and $\sigma^{(\max)}(E_\gamma) = \sigma^{(9)}(E_\gamma)$ results for Ta. Remainder of caption as in fig. 3.

measured $\sigma^{(9)}$, $\sigma^{(10)}$ and even $\sigma^{(11)}$ separately, but their values were found to be too small to be significant. Our actual experimental conditions are such that, in the Ce case, we can only measure $\sigma^{(j)}(E_\gamma)$ values of roughly 1 mb for $j \geq 5$ and therefore only physically meaningful measurements are shown.

4.3. THE U DATA

One finds that the experimental uncertainties for the uranium case are much larger because large background corrections have to be made. The radioactive U target produced an intense gamma-ray background, which unfortunately, was also detected by the liquid scintillator of the 4π neutron detector. Nevertheless, data are presented in the same way as for the previously shown nuclei. The $\sigma^{(2)}(E_\gamma)$ and $\sigma^{(\max)}(E_\gamma) = \sigma^{(12)}(E_\gamma)$ data, shown in fig. 7, are connected by solid lines representing the "smoothed" average through the error bar weighted experimental points.

5. The case of the $\sigma^{(1)}$ data

The measurements of $\sigma^{(1)}$ are particularly hampered by large statistical and systematic uncertainties. Even though the use of photon spectra at $\theta = 4°$, shown in

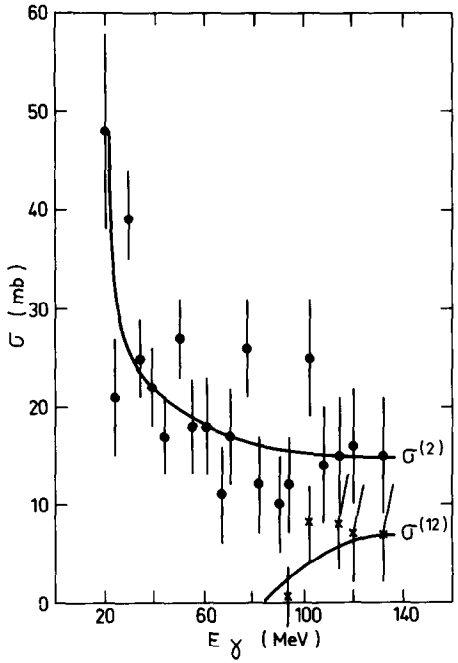

Fig. 7. Experimental $\sigma^{(2)}(E_\gamma)$ and $\sigma^{(\max)}(E_\gamma) = \sigma^{(12)}(E_\gamma)$ results for U. Remainder of caption as in fig. 3 but no intermediate $\sigma^{(j)}(E_\gamma)$ plots are shown at all.

fig. 1, decreases the number of bremsstrahlung photons, the photons remaining in the energy range around the GDR still produce many $\sigma(\gamma, n)$ events since $\sigma(\gamma, n) >$ 400 mb for Pb and 11 MeV $\leq E_\gamma \leq$ 15 MeV. Therefore the $\sigma^{(1)} - \sigma^{(2)}$ contribution, which will be shown to be <5 mb for Pb at $E_\gamma = 100$ MeV, will show up as a very small fractional difference between two large numbers, $[N^{(1)}_{LiH} - RN^{(1)}_{Cu}]$, and therefore will be beset with large statistical errors [which have been discussed elsewhere [12])].

A more troublesome and systematic error arises from what remains in our method of photoatomic effects which make the Mainz method inapplicable for heavy nuclei. If we work with a 2 mm thick Pb target, approximately 10% of the monochromatic photons will produce $e^+ - e^-$ pairs in the first half of this Pb target. These pairs can, in turn, produce low-energy bremsstrahlung photons in the second half of the Pb target, or even in the rear part of the neutron detector itself, if their angular distribution is made wide enough by multiple scattering in the thick photonuclear target. These low-energy "target-produced" bremsstrahlung photons can produce spurious GDR (γ, 1n) events which might be wrongly attributed to the nuclear absorption of the monochromatic photons in the target.

Since such spurious (γ, 1n) effects should clearly decrease with the target thickness t, we carried out several measurements at a fixed E_γ with targets of variable thickness. The assumption was that, by extrapolating the measured $\sigma^{(1)}(E_\gamma, t)$ and $\sigma^{(2)}(E_\gamma, t)$ values towards $t = 0$, one should get the true $\sigma^{(1)}(E_\gamma) - \sigma^{(2)}(E_\gamma)$ difference. Since the use of very thin targets made such experiments very time consuming, these measurements were therefore carried out only for a few sampled values of the energy E_γ. Table 2 shows the results obtained for Pb, and summarizes the detailed data

TABLE 2

Measured $\sigma^{(1)}(E_\gamma) - \sigma^{(2)}(E_\gamma)$ values for Pb at various photon energies E_γ (see also figs. 8 and 9)

E_γ (MeV)	$\sigma^{(1)} - \sigma^{(2)}$ (mb)
24	1.5±4
27	−1±4
33	3.5±4
40	3.5±4
45	6±4
58	1±4
82	1±4
103	9±4

represented in fig. 8. The shape of the solid lines in fig. 8, which fit the experimental points and allow the extrapolation towards the $\sigma^{(1)}$ value for $t = 0$, results from the combination of two spurious effects. The first one produces a "spurious (γ, n) cross section" in the target itself and varies as t^2. The second one produces a "spurious

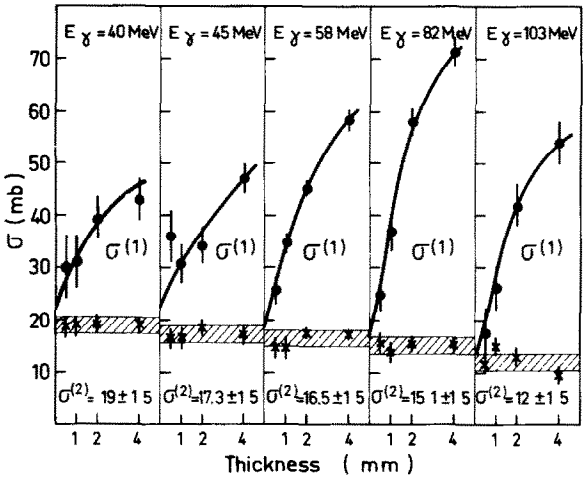

Fig. 8. The $\sigma^{(1)}(E_\gamma, t)$, ■ and $\sigma^{(2)}(E_\gamma, t)$, ✳ data, measured at $E_\gamma = 40$ MeV, 45 MeV, 58 MeV, 82 MeV and 103 MeV for Pb. For each energy, E_γ, four measurements were carried out with Pb targets of thicknesses $t = 0.5$ mm, 1 mm, 2 mm and 4 mm (see also table 2).

(γ, n) cross section" in the rear part of the neutron detector, and depends mostly on the multiple scattering angle of the electron and positron pairs in the target, which varies as $\sqrt{t}$.

One observes that $\sigma^{(1)} \simeq \sigma^{(2)}$ within the error bars given for $\sigma^{(2)}$ in fig. 2 (or 3). However, there probably is a small positive $\sigma^{(1)} - \sigma^{(2)}$ contribution between 30 and 60 MeV which is represented by the difference between the dotted and solid lines in fig. 9.

When one uses the $\sigma^{(1)} - \sigma^{(2)}$ values of table 2 one finds that

$$\int_{30\,\mathrm{MeV}}^{140\,\mathrm{MeV}} [\sigma^{(1)}(E_\gamma) - \sigma^{(2)}(E_\gamma)]\,\mathrm{d}E_\gamma \leq 4 \times 10^{-2} \sigma_0\,,$$

whereas Wu and Chang predicted $\simeq 1 \times 10^{-2} \sigma_0$ for the above integral. Moreover, the most likely behaviour of $\sigma^{(1)}$, shown by the dotted line in fig. 14, suggests that one may observe some (γ, np) contributions above 30 MeV, i.e. for energies larger than "B_{np} + Coulomb barrier". This contribution would slowly disappear when the average multiplicity of the emitted nucleons increases with E_γ. Exactly the same conclusions were reached experimentally for the Sn, Ce and Ta nuclei. For each of these three nuclei too, four samples with different thicknesses were used at some sampled energies and $\sigma^{(1)}(E_\gamma) - \sigma^{(2)}(E_\gamma)$ was found to be $= 0$ within the error bars $\Delta\sigma^{(2)}(E_\gamma)$ for $E_\gamma > 60$ MeV. The integrated value of the possible contribution was also found to be $\leq 4 \times 10^{-2} \sigma_0$.

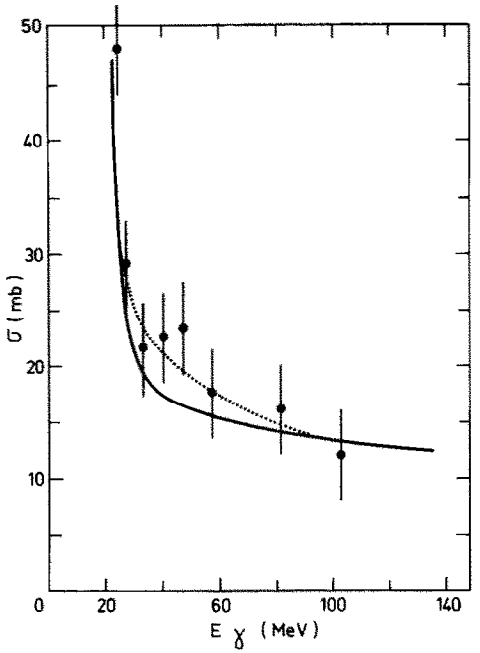

Fig. 9. Comparison of the measured $\sigma^{(1)}(E_\gamma)$ and $\sigma^{(2)}(E_\gamma)$ data for Pb. The solid line is the smoothed averaged $\sigma^{(2)}(E_\gamma)$ curve already represented in figs. 2a and 3. The dotted line is drawn through the experimental $\sigma^{(1)}(E_\gamma)$ points taken from table 2.

6. Comparison of available data

Since Jones and Terwilliger [3]) did not measure the photoneutron multiplicities $\nu(E_\gamma)$, they could only evaluate neutron yield cross sections $\sigma(\gamma, x\mathrm{n}) = \sum_i i\sigma(\gamma, i\mathrm{n})$. Our experimental procedure, however, allows us to obtain total photonuclear cross sections $\sigma(\mathrm{tot}: E_\gamma) \simeq \sum_i \sigma(\gamma, i\mathrm{n}: E_\gamma)$ *directly*. Nevertheless, one can also extract photoneutron yield cross sections $\sigma(\gamma, x\mathrm{n})$ from our experimental raw data for the sole purpose of comparing them with the earlier Jones–Terwilliger results. Since we found that $\sigma^{(1)}(E_\gamma) \simeq \sigma^{(2)}(E_\gamma)$ we therefore computed $\sigma(\gamma, x\mathrm{n})$ by means of the following expression

$$\sigma(\gamma, x\mathrm{n}) = \sum_i i\sigma(\gamma, i\mathrm{n}) = \sum_{j=1} \sigma^{(j)}(E_\gamma)\,,$$

where the first term $\sigma^{(1)}(E_\gamma)$ was replaced by its near equivalent $\sigma^{(2)}(E_\gamma)$.

Data from ref. [3]) and our results for Pb are compared in fig. 10, where the dotted line, representing the Jones–Terwilliger data, is rather uncertain since it had to be extracted from the figures shown in their publication.

Moreover, the authors also state in their paper [3]) that "the shape of the $\sigma(\gamma, x\mathrm{n})$ curves is probably good only to within ±30%". But even when one takes the above

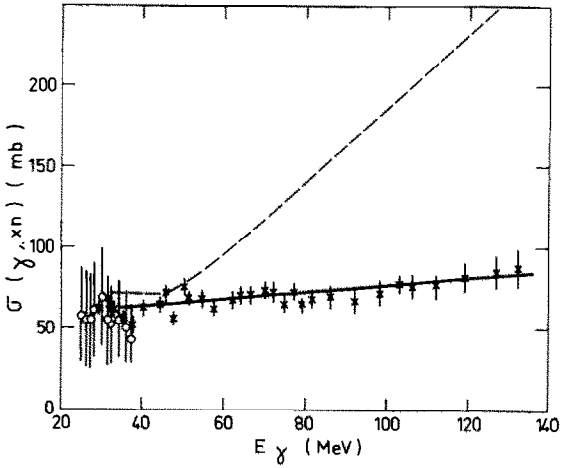

Fig. 10. Comparison between the Jones–Terwilliger photoneutron yield cross sections $\sigma(\gamma, x\mathrm{n})$, taken from ref. [3]) and indicated by the dashed line, and recent Saclay data, represented by the full line, for Pb and photon energies E_γ between 20 and 140 MeV. The ⋇ Saclay data are from this paper but the ⌀ results were evaluated from previously published [5]) Saclay results covering the GDR photon energy region.

remarks into account, it is quite obvious from fig. 10 that our new $\sigma(\gamma, x\mathrm{n})$ Saclay data do not exhibit the pronounced increase with photon energy E_γ, clearly shown by the older Jones–Terwilliger results. Moreover, the average behaviour of $\sigma(\gamma, x\mathrm{n})$ as a function of E_γ, for the four other nuclei studied, is quite similar as shown in fig. 11.

One can also extract neutron yield cross sections $\sigma(\gamma, x\mathrm{n})$ from earlier Saclay measurements of the partial photoneutron cross sections $\sigma(\gamma, \mathrm{n})$, $\sigma(\gamma, 2\mathrm{n})$, $\sigma(\gamma, 3\mathrm{n})$ and $\sigma(\gamma, 4\mathrm{n})$ for Pb and photon energies E_γ in the giant dipole resonance (GDR)

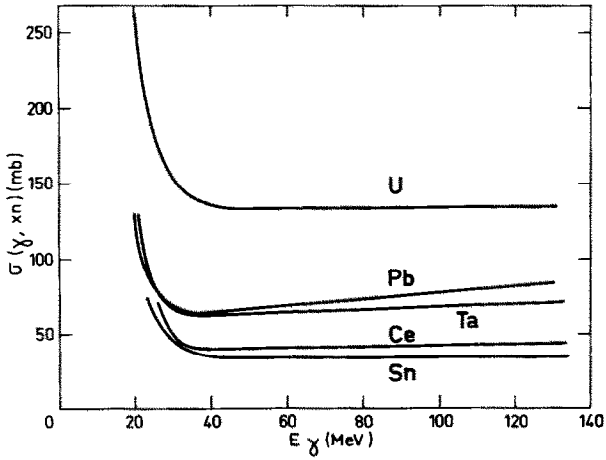

Fig. 11. The general behaviour of the "smoothed" average neutron yield cross sections $\sigma(\gamma, x\mathrm{n}) = \sum_i i\sigma(\gamma, i\mathrm{n}; E_\gamma)$ for the Sn, Ce, Ta, Pb and U nuclei studied in the present paper (see text).

region of ($7\,\mathrm{MeV} \leq E_\gamma \leq 35\,\mathrm{MeV}$). These measurements were made at a photon emission angle of $\theta = 0°$ (not $\theta = 4°$ as is actually the case) and this implies a much larger contribution [12]) of bremsstrahlung photons. Such a large bremsstrahlung contamination in turn means fairly large uncertainties in the evaluation of $\sigma(\gamma, xn)$ for the upper part of the GDR above $E_\gamma \approx 20\,\mathrm{MeV}$ say. Nonetheless, one sees from fig. 10, that one obtains reasonable agreement between the old and the new Saclay $\sigma(\gamma, xn)$ yield data.

Our total photonuclear cross sections $\sigma(\mathrm{tot}: E_\gamma) \approx \sigma^{(2)}(E_\gamma)$ can also be compared with the sum of the partial photoneutron cross sections which were measured at Lund [6]) for ^{197}Au and ^{127}I. One observes in fig. 12 that our $\sigma^{(2)}(E_\gamma)$ data are significantly larger than the Lund data. This is of course normal since they studied only a few of the possible decay channels. However it is worth noticing that their "cross sections" decrease slowly above $E_\gamma \sim 50\,\mathrm{MeV}$ in good agreement with our results.

As to our own $\sigma^{(2)}(E_\gamma)$ results, in fig. 12 one clearly notices the regular and expected increase of $\sigma^{(2)}(E_\gamma)$ with the mass number A, a point which will be quantitatively examined in the section concerning the sum rules.

7. The integrated cross section and the E1 sum rule

One can also compare theoretical sum rule evaluations, which have been made for the electric dipole E1 sum rule, with integrated cross-section values extracted from

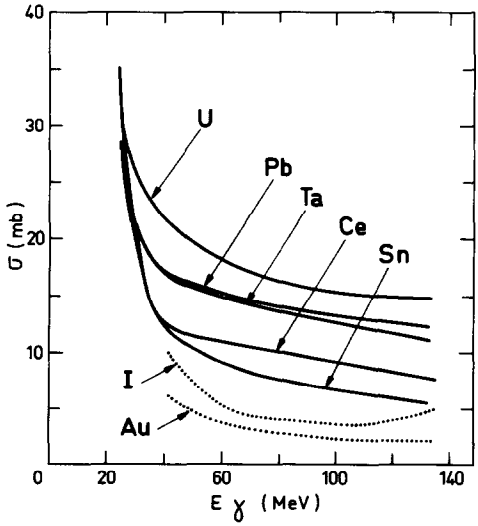

Fig. 12. A comparison between the sum of certain partial photoneutron cross sections, measured at Lund [6]) for ^{197}Au and ^{127}I and represented by the dotted curves, and the total photonuclear absorption cross section $\sigma(\mathrm{tot}: E_\gamma) \approx \sigma^{(2)}(E_\gamma)$ for Pb, Sn, Ce, Ta and U obtained in this paper and represented by the full line plots.

the above experimental data. If one calls $\sigma_\gamma^{E1}(E_\gamma)$ the total E1 photoabsorption cross section one is interested in getting the value $\Sigma_0(\mathrm{E1})$

$$\Sigma_0(\mathrm{E1}) = \int \sigma_\gamma^{E1}(E_\gamma)\,\mathrm{d}E_\gamma = \frac{4\pi^2}{\hbar c}\sum_f (E_f - E_0)|\langle\psi_f|D_z|\psi_0\rangle|^2\rho_f$$

$$= \frac{2\pi^2}{\hbar c}\langle\psi_0|[D_z,[H_N, D_z]]|\psi_0\rangle\,,$$

where $E_\gamma = E_f - E_0$, $|\psi_0\rangle$ is the nuclear ground-state wave function, $|\psi_f\rangle$ is the nuclear final-state wave function, ρ_f is the density of the nuclear final states, H_N is the nuclear hamiltonian, $D_z = \sum_i \frac{1}{2}e(1+\tau_z(i))z_i$ is the dipole operator. When $[V, D_z] = 0$, where $V = \sum_{i<j} V(i,j)$ is the two-body nucleon–nucleon potential,

$$\Sigma_0(\mathrm{E1}) = \sigma_0 = 2\pi^2\,e^2\,\frac{\hbar}{mc}\,\frac{NZ}{A} = 0.06\,\frac{NZ}{A}\,\mathrm{MeV}\cdot\mathrm{b}\,,$$

which is the classical Thomas–Reiche–Kuhn evaluation of the electric dipole sum rule for the ${}_ZA_N$ nucleus.

However, if exchange forces are present, additional terms contribute to the double commutator, and it is convenient to express $\Sigma_0(\mathrm{E1})$ as follows: $\Sigma_0(\mathrm{E1}) = \sigma_0(1+K)\,\mathrm{MeV}\cdot\mathrm{b}$ where the enhancement factor, K, can be written as

$$K = \frac{mA}{e^2\hbar^2 NZ}\langle\psi_0|[D_z,[V, D_z]]|\psi_0\rangle\,.$$

In the dipole approximation a determination of K is a global measure of the exchange component (or the momentum-dependent part) of the nuclear force.

Now the question arises: which experimental number should be compared to the calculated $\Sigma_0(\mathrm{E1})$ sum rule? Ziegler [23]) and Arenhövel [24]) recently wrote critical reviews of this problem where two main points have to be considered.

(a) The measured $\sigma(\mathrm{tot}: E_\gamma)$ values include multipoles other than E1. But one can show [23]) that for heavy nuclei, less than $0.06\int\sigma(\mathrm{tot}: E_\gamma)\,\mathrm{d}E_\gamma$ corresponds to Eλ transitions with $\lambda \neq 1$.

Fortunately, as has been shown by Gerasimov, the relatively small increase in the experimental integrated cross section, which is due to $\lambda \neq 1$ multipoles is fairly well compensated by the retardation effects [25]).

(b) There still remains the problem that the integration of $\sigma(\mathrm{tot}: E_\gamma)$ has to be carried out up to some reasonable upper limit. If one wants to make a comparison with conventional theories, namely those which evaluate $\Sigma_0(\mathrm{E1})$ without the inclusion of isobar excitations, it is then reasonable to make such comparisons with the experimental values $\sigma(\mathrm{tot}: E_\gamma)$ integrated up to $m_\pi = 140$ MeV and one can thus write:

$$\int_{B_{1n}}^{140\,\mathrm{MeV}} \sigma(\mathrm{tot}: E_\gamma)\,\mathrm{d}E_\gamma = \sigma_0(1+K)\,.$$

The corresponding data are summarized in table 3 and in fig. 13. The points plotted

TABLE 3

Integrated cross sections

	Sn	Ce	Ta	Pb	U	U
$\sigma_0 = 0.06NZ/A$ (MeV · b)	1.74	2.04	2.61	2.97	3.40	3.40
$E_{\gamma 0}$(MeV)	29.7	25	25	25	18	18.30
$M = \int_{B_{1n}}^{E_{\gamma_0}} \sigma_{GDR}(E_\gamma)\, dE_\gamma$ (MeV · b)	2.0 ± 0.15 [a]	2.13 ± 0.15 [b]	2.90 ± 0.23 [b]	3.48 ± 0.23 [c]	2.98 ± 0.15 [d]	3.58 [e]
(σ_0 unit)	1.15 ± 0.09	1.04 ± 0.07	1.11 ± 0.09	1.17 ± 0.08	0.88 ± 0.05	1.05
$N = \int_{E_{\gamma 0}}^{140\ \mathrm{MeV}} \sigma^{(2)}(E_\gamma)\, dE_\gamma$ (Mev · b)	0.96 ± 0.1	1.27 ± 0.1	1.73 ± 0.15	1.69 ± 0.15	2.59 ± 9.2	2.59 ± 0.2
(σ_0 unit)	0.55 ± 0.06	0.63 ± 0.05	0.66 ± 0.06	0.57 ± 0.05	0.76 ± 0.06	0.76 ± 0.06
$M+N$ (MeV · b)	2.96 ± 0.2	3.40 ± 0.2	4.63 ± 0.3	5.17 ± 0.3	5.57 ± 0.3	6.17 ± 0.3
(σ_0 unit)	1.70 ± 0.12	1.67 ± 0.10	1.77 ± 0.10	1.74 ± 0.10	1.64 ± 0.10	1.81 ± 0.10
$(M+N)$ + evaluation of the $\int_{E_{\gamma 0}}^{140\ \mathrm{MeV}} \lvert\sigma^{(1)} - \sigma^{(2)}\rvert\, dE_\gamma$ contribution $= (1+K)$ (σ_0 unit)	1.74 ± 0.15	1.71 ± 0.15	1.81 ± 0.15	1.78 ± 0.15	1.68 ± 0.15	1.85 ± 0.15
$\int^{m_\pi} \sigma_L(E_\gamma)\, dE_\gamma$ (σ_0 unit)	1.28 [a]	1.24 [b]	1.30 [b]	1.35 [a]	1.18 [d]	1.43 [e]

[a]) Ref. [26]). [b]) Ref. [27]). [c]) Ref. [5]). [d]) Ref. [28]). [e]) Ref. [29]).

The symbols M and N are defined in the text. The last row gives the integrated cross sections for the Lorentz line fit, $\sigma_L(E_\gamma)$ to the GDR data, published in the above references.

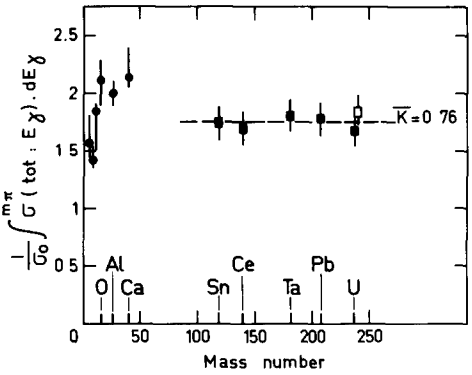

Fig. 13. The integrated experimental cross sections, $\int_{B_{1n}}^{140\,\mathrm{MeV}-m_\pi} \sigma(\mathrm{tot}:E_\gamma)\,\mathrm{d}E_\gamma$ in units of σ_0 (see table 3). The full squares combine the GDR data previously obtained at Saclay [26,27,5,28]), with the present measurements covering energies between 30 and 140 MeV. The uranium measurement is shown twice. The second value, plotted as an open square, uses the GDR data recently obtained at Livermore [29]). The ● circular points were obtained at Mainz [1]) by the total absorption method.

as squares represent our recommended integrated experimental cross sections, which were obtained from

$$\int_{B_{1n}}^{140\,\mathrm{MeV}} \sigma(\mathrm{tot}:E_\gamma)\,\mathrm{d}E_\gamma \simeq M + N + 4\times10^{-2}\sigma_0\,.$$

Here,

$$M = \int_{B_{1n}}^{E_{\gamma 0}} \sigma_{\mathrm{GDR}}(\mathrm{tot}:E_\gamma)\,\mathrm{d}E_\gamma\,,$$

and $\sigma_{\mathrm{GDR}}(\mathrm{tot}:E_\gamma)$ is the photonuclear cross section, measured in the GDR region, which was taken to be equal to either:

$$\sigma_{\mathrm{GDR}}(\mathrm{tot}:E_\gamma) \simeq \sigma(\gamma,\,1\mathrm{n}) + \sigma(\gamma,\,2\mathrm{n}) + \sigma(\gamma,\,3\mathrm{n})$$

for Sn [ref. [26])], Ce, Ta [ref. [27])] and Pb [ref. [5])] (previous Saclay measurements) or:

$$\sigma_{\mathrm{GDR}}(\mathrm{tot}:E_\gamma) \simeq \sigma(\gamma,\,1\mathrm{n}) + \sigma(\gamma,\,2\mathrm{n}) + \sigma(\gamma,\,\mathrm{fission})\,.$$

for U [Saclay [28]) or Livermore [29]) previous measurements]. Finally, we put

$$N = \int_{E_{\gamma 0}}^{140\,\mathrm{MeV}} \sigma^{(2)}(E_\gamma)\,\mathrm{d}E_\gamma$$

where $\sigma^{(2)}(E_\gamma)$ are the newly measured data presented in this paper. The $4\times10^{-2}\sigma_0$ term is our best measurement of the $\int_{E_{\gamma 0}}^{140\,\mathrm{MeV}} [\sigma^{(1)}(E_\gamma) - \sigma^{(2)}(E_\gamma)]\,\mathrm{d}E_\gamma$ contribution from the $(\gamma,\,1\mathrm{n})$ and $(\gamma,\,1\mathrm{p}\,1\mathrm{n})$ channels. Since our best knowledge of the contribution of the $(\gamma,\,\mathrm{p})$, $(\gamma,\,2\mathrm{p})$, . . . channels to the integrated cross section can be evaluated

to be smaller than $5\times10^{-2}\sigma_0$, it is clear that the error bars shown in fig. 13 largely include this small (and yet unmeasured) contribution. On the same figure 13 the Mainz values for Li, Be, C, O and Ca nuclei [1]) are also represented with error bars including both statistical and systematic errors. It might be worth noticing that these Mainz values, and their corresponding error bars, may have to be slightly modified if one wants to use more recent and perhaps more precise evaluations [8,30]) of the total atomic cross sections, $\sigma_{\mathrm{tot\,A}}(E_\gamma)$.

One is thus led to the conclusion that the average enhancement factor, $\bar{K}$, for the 5 heavy nuclei, Sn, Ce, Ta, Pb and U, has a value of

$$\bar{K}=0.76\pm0.10\,.$$

Moreover, K seems to be quite independent of A over the $119<A<238$ range (i.e. a factor of 2 in A). One notices further that this average $\bar{K}=0.76$, would agree with an average K-value taken from the Mainz data only. Finally, our $\bar{K}=0.76$ result is about twice the value often quoted about ten years ago, when an integration up to $E_\gamma=m_\pi$ of the Lorentz line, fitting the GDR data, was considered to be reasonable. As shown in the last row of table 3, such a procedure leads to $K\simeq0.30$.

A large value for K ($\simeq1$) has been predicted theoretically by Arima *et al.* [31]), Weng *et al.* [32]) and Gari *et al.* [33]) and is mostly due to the tensor interactions. In order for these to contribute fully, tensor correlations must be considered in the nuclear ground state $|\psi_0\rangle$ used to evaluate the expectation value of the double commutator. Similar theoretical estimates of the enhancement factor K were recently published by Sandler and Clark [34]), who have calculated this number for symmetrical correlated nuclear matter at $k_f\simeq1.2\ \mathrm{fm}^{-1}$, and their results ($K=0.72$ for the Hamada–Johnston or $K=0.89$ for the Gammel–Christian–Thaler interaction) confirm the importance of tensor correlations.

Recently, Brown and Rho [35]) divided K into two parts, $K=K_1+K_2$. The first, K_1, should show up in the integrated cross section in the GDR region, (say up to 25 MeV) and has been connected by Fujita [36]) to δ_{g_l}, the change in the nucleonic g-factor arising from exchange currents. Our results, quoted in the third row of table 3, would lead to an experimental value (averaged over Sn to U) of:

$$\int_{B_{1n}}^{25\ \mathrm{MeV}}\sigma_{\mathrm{GDR}}(\mathrm{tot}:E_\gamma)\,\mathrm{d}E_\gamma=\sigma_0(1+K_1)\quad\text{with } K_1\simeq0.12\pm0.05\,.$$

Such a value does not disagree with the statement of Brown and Rho that their model predicts a small (probably less than 0.2) K_1 value when the total photonuclear cross sections are integrated up to 25 MeV, a reasonable, albeit somewhat arbitrary cut off energy for the GDR region. The second part, K_2, should be mainly due to the effect of the tensor force and tensor correlations which involve high virtual momenta. Hence their contribution should be found above the GDR in the $25\ \mathrm{MeV}<E_\gamma<140\ \mathrm{MeV}$ region, where another mechanism, the "quasideuteron effect", is expected

to be mostly responsible for the photon absorption [37]). Our results thus lead to the value $K_2 = 0.64 \pm 0.10$.

8. The energy dependence of $\sigma(\text{tot}: E_\gamma)$ and the quasideuteron effect

One may study the quasideuteron effect by studying the E_γ dependence of $\sigma(\text{tot}: E_\gamma)$. Fig. 14 shows how the Lorentz line $\sigma_L(E_\gamma)$, used to fit the GDR data, provides a very good fit to the experimental data [5]) up to $E_\gamma = 25$ MeV for the Pb case. For $E_\gamma > 25$ MeV, one observes that $\sigma(\text{tot}: E_\gamma) > \sigma_L(E_\gamma)$, and for $E_\gamma = 40$ MeV

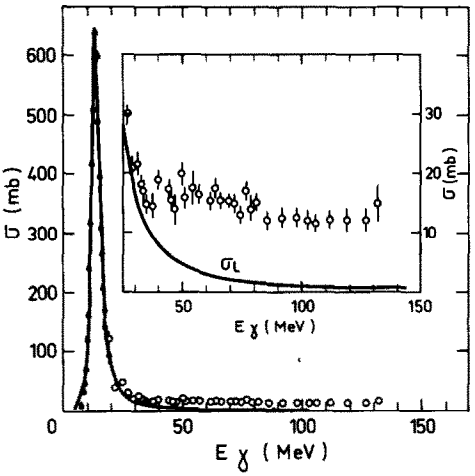

Fig. 14. Total photonuclear absorption cross-section data $\sigma(\text{tot}: E_\gamma)$ for Pb. Results obtained in the GDR region are represented by triangular points and come from ref. [5]). The circular data points cover the 30 to 140 MeV photonenergy range and are taken from the present paper. Both data sets are compared with a Lorentz curve $\sigma_L(E_\gamma)$ fitted only to the GDR photonuclear data of ref. [5]), but extrapolated to $E_\gamma =$ 140 MeV.

one has $\sigma(\text{tot}: E_\gamma) \simeq 3\sigma_L$. Clearly, the resonant behaviour described by $\sigma_L(E_\gamma)$ does not fit our experimental $\sigma(\text{tot}: E_\gamma)$ data for Pb which show, from 40 to 140 MeV, a non-resonant and smoothly decreasing shape, similar to the "average" shape of the $\sigma(\text{tot}: E_\gamma)$ data already obtained at Mainz for light nuclei. A similar behaviour for Sn, Ce, Ta and U nuclei is also shown in fig. 15 where the corresponding $\sigma_L(E_\gamma)$ parameters were taken from refs. [5,26–28]), respectively.

For the lightest nuclei (Li, Be, C, O), the Mainz data could be roughly fitted for $50\ \text{MeV} < E_\gamma < 140\ \text{MeV}$ by using the initial formulation of Levinger [2]) for the absorption of short wavelength photons by correlated neutron–proton pairs in the quasideuteron model namely

$$\sigma(\text{tot}: E_\gamma) \simeq L \frac{NZ}{A} \sigma_D(E_\gamma) = \sigma_{QD}(E_\gamma) ,$$

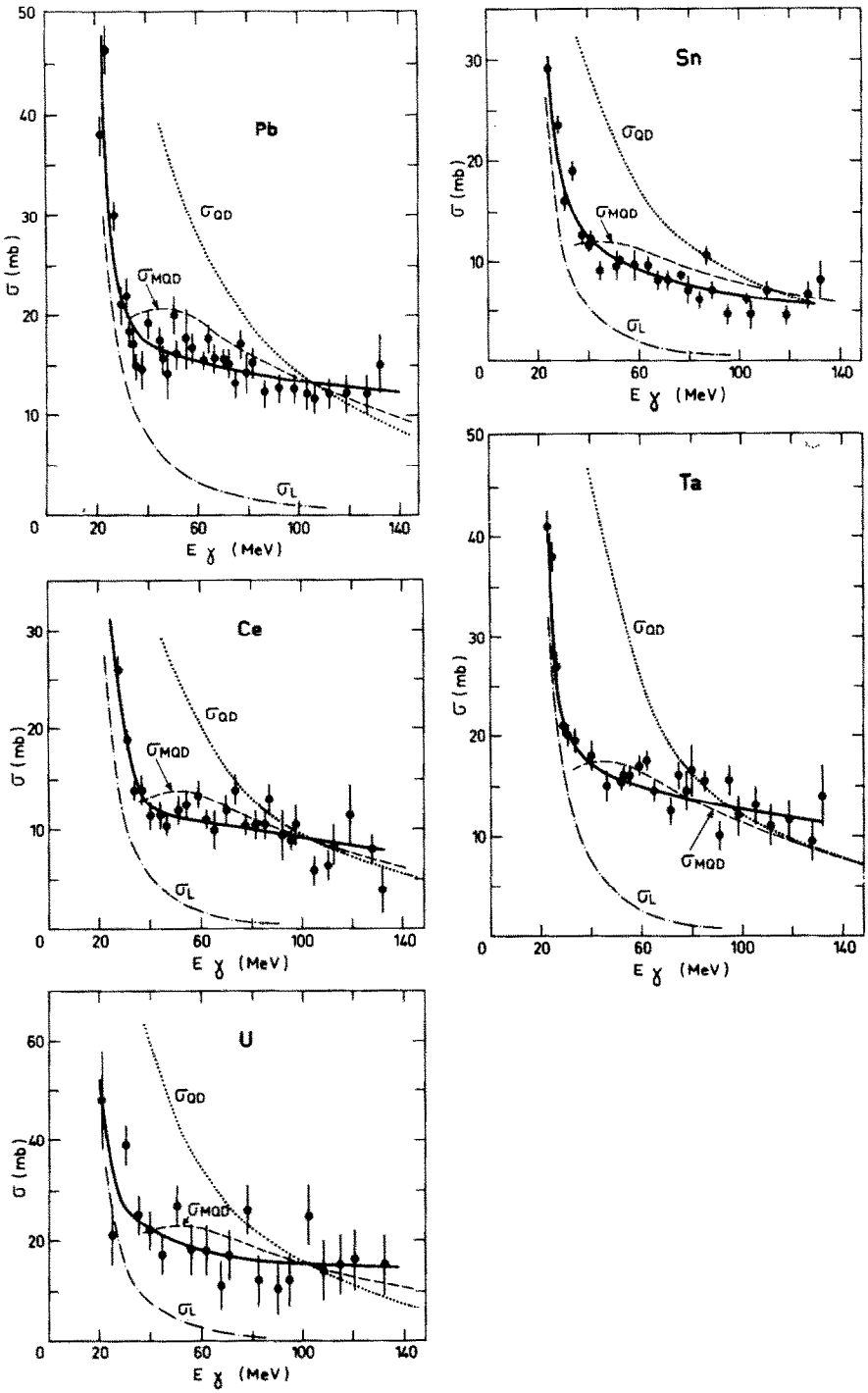

Fig. 15. Total photonuclear absorption cross sections $\sigma(\text{tot}:E_\gamma) \approx \sigma^{(2)}(E_\gamma)$ from the present paper, represented by the experimental points and the corresponding full lines, are shown for Pb, Sn, Ce, Ta and U. These experimental results for photon energies E_γ between 20 and 140 MeV are compared with: (a) Lorentz line fits to the GDR data of the appropriate nucleus represented by the dot-dash $\sigma_L(E_\gamma)$ plots. (b) Quasideuteron cross sections, $\sigma_{QD}(E_\gamma) = (4.6NZ/A)\sigma_D(E_\gamma)$ for the appropriate nuclei, represented by the dotted $\sigma_{QD}(E_\gamma)$ plots. Here $\sigma_D(E_\gamma)$ is the photodisintegration cross section of deuterium. (c) Modified quasideuteron cross sections, $\sigma_{QDM}(E_\gamma) = (8NZ/A)\sigma_D(E_\gamma) \exp(-D/E_\gamma)$ with $D = 60$ MeV, represented by the dashed $\sigma_{MQD}(E_\gamma)$ plots. Pertinent GDR data for Pb, Sn, Ce, Ta and U were taken from refs. [5,26–28]).

where $\sigma_D(E_\gamma)$ is the deuteron photodisintegration cross section, $L = 4.6 \pm 0.5$ is the value of the best Mainz fit for Li and Be, and NZ/A is the effective number of quasideuterons which can take part in the photoabsorption.

Clearly, fig. 15 also shows that the above σ_{QD} expression evaluated with $L = 4.6$, cannot fit our $\sigma(\text{tot}: E_\gamma)$ data, at least below 100 MeV.

Hence, some modification has to be introduced into the classical quasi-deuteron model. In order to get a more precise view of the possible A-dependence for any such modified model, one can first try to achieve an approximate separation between the "quasideuteron absorption" and what remains, above $E_\gamma \sim 40$ MeV, of the "GDR volume oscillation effect" assumed to be represented by the extrapolated $\sigma_L(E_\gamma)$ values. In fig. 16 we represent the ratios

$$\frac{\sigma(\text{tot}: E_\gamma) - \sigma_L(E_\gamma)}{NZ\sigma_D(E_\gamma)/A},$$

where our smoothed average $\sigma^{(2)}(E_\gamma)$ data represent $\sigma(\text{tot}: E_\gamma)$. Clearly, the same behaviour is exhibited by the five nuclei represented. Hence, the required modification of the original quasideuteron model should not be dependent upon A. Two such modifications have been recently proposed by Levinger and Laget.

In order to obtain a better fit with his model over a larger energy range (especially below 100 MeV), Levinger recently pointed out that another phenomenon has to be taken into account for photon energies comparable to the Fermi energy in the nucleus. Then, Pauli blocking for the neutron (or proton), emitted from the quasi-deuteron which absorbs the photon, should lead to some important damping of the σ_{QD} cross section. Levinger represented the effect of such damping by means of an exponential factor so that one should now try to fit $\sigma(\text{tot}: E_\gamma)$ by the modified quasideuteron cross section [38]):

$$\sigma_{MQD}(E_\gamma) \simeq L \frac{NZ}{A} \exp\left(-\frac{D}{E_\gamma}\right) \sigma_D(E_\gamma).$$

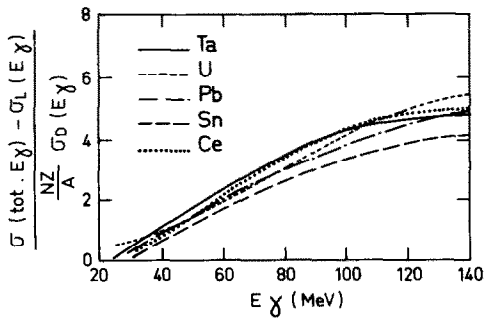

Fig. 16. Normalized $[\sigma(\text{tot}: E_\gamma) - \sigma_L(E_\gamma)]/[NZ\sigma_D(E_\gamma)/A]$ values for Pb, Sn, Ce, Ta and U. The $\sigma(\text{tot}: E_\gamma) \approx \sigma^{(2)}(E_\gamma)$ data are those shown in figs. 3 to 7, the $\sigma_L(E_\gamma)$ results come from fig. 15 and $\sigma_D(E_\gamma)$ is the photodisintegration cross section of deuterium.

As shown in fig. 15 our experimental data for $40\,\text{MeV} < E_\gamma < 140\,\text{MeV}$ give a reasonable fit to the above formula for $L = 8$ and $D = 60\,\text{MeV}$ i.e. in the region where the extrapolated $\sigma_L(E_\gamma)$ values become much smaller than $\sigma(\text{tot}:E_\gamma)$.

However, it is not easy to give a theoretical evaluation of the damping factor D, and other combinations for the numerical values of L and D might also lead to reasonable fits of our experimental data.

More recently, Laget suggested another explanation for the different behaviour of $\sigma(\text{tot}:E_\gamma)$ and $NZ\sigma_D/A$. He proposed associating the absorption of a 40 to 140 MeV photon by a quasideuteron, only with the exchange part, $\sigma_D^{\text{exch}}(E_\gamma)$, in the total photodisintegration cross section $\sigma_D(E_\gamma)$ of the deuterium.

In the deuteron case, $\sigma_D^{\text{exch}}(E_\gamma)$ corresponds to the transition amplitude where a virtual meson is emitted by a nucleon and then reabsorbed by the other nucleon of the deuteron. Laget [39]) has computed these $\sigma_D^{\text{exch}}(E_\gamma)$ values, which are summarized in table 4 together with the classical values for the total photodisintegration of the deuterium, $\sigma_D(E_\gamma)$.

TABLE 4

The $\sigma_D^{\text{exch}}(E_\gamma)$ cross section, computed by Laget [39]), and the corresponding values of the classical total photodisintegration cross section of deuterium, $\sigma_D(E_\gamma)$ for photons between 20 and 140 MeV

E_γ (Mev)	20	30	40	50	80	100	120	140
$\sigma_D(E_\gamma)$ (μb)	590	370	231	154	88	70	62	54
$\sigma_D^{\text{exch}}(E_\gamma)$ (μb)	38.8	37.5	33.8	31.2	25.5	23.2	21.6	20.7
$\dfrac{\sigma_D^{\text{exch}}(E_\gamma)}{\sigma_D(E_\gamma)}$	0.066	0.101	0.159	0.203	0.290	0.331	0.348	0.383

The behaviour of the $\sigma_D^{\text{exch}}(E_\gamma)/\sigma_D(E_\gamma)$ ratio, given in table 4, shows a good qualitative similarity with our average experimental increase with E_γ of the ratio

$$\frac{\sigma(\text{tot}:E_\gamma) - \sigma_L(E_\gamma)}{NZ\sigma_D(E_\gamma)/A}$$

shown in fig. 16. The experimental $\sigma(\text{tot}:E_\gamma) \simeq \sigma^{(2)}(E_\gamma)/(NZ/A)$ results for Sn, Ce, Ta and Pb, normalized to NZ/A, are shown in fig. 17. Surprisingly, all points lie on a "universal" curve represented by

$$\sigma(\text{tot}:E_\gamma) = (11 \pm 2)\frac{NZ}{A}\sigma_D^{\text{exch}}(E_\gamma),$$

and this even without having taken any Pauli effect into account.

In this approach, the "universal" increase with E_γ, experimentally observed in fig. 16, would no longer be connected to the disappearance of a Pauli blocking effect but rather to an increase of the $\sigma_D^{\text{exch}}(E_\gamma)/\sigma_D(E_\gamma)$ ratio.

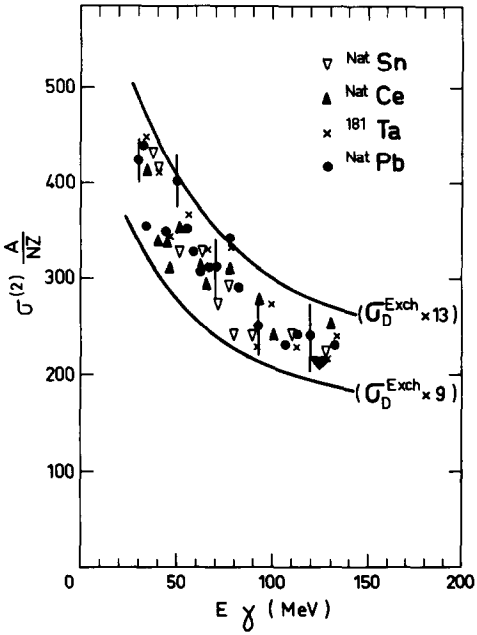

Fig. 17. Experimental $\sigma^{(2)}(E_\gamma)A/NZ = \sigma(\text{tot}: E_\gamma)A/NZ$ results for Sn, Ce, Ta and Pb are compared with values proportional to the theoretical evaluations of $\sigma_D^{exch}(E_\gamma)$, (full lines), computed by Laget [39]).

This last interpretation, together with the fundamental result for the so-called enhancement factor K in the dipole sum, suggest rather strongly that the exchange of mesons between the nucleons in nuclei corresponds to a very physical picture [23,35]).

In other words, and according to the physical meaning of the Gell-Mann–Goldberger–Thirring sum rule, the exchange part of the nuclear forces increases the photoabsorption below the pion threshold, by effectively increasing the number of charges responsible for the absorption, and that same exchange part reduces the pion photoproduction cross section of A free particles, in the isobar resonance region, when they become bound together in a nucleus. This is what was actually observed for lithium and beryllium in the limited energy range $E_\gamma < 330$ MeV covered so far by the Mainz group [40]).

These contributions to the understanding of photonuclear reactions at intermediate energies, strongly suggest the extension of such measurements of $\sigma(\text{tot}: E_\gamma)$ to higher energies for a series of medium and heavy nuclei.

We would like to thank J. Levinger and J.M. Laget for their explanations concerning the possible modifications of the quasi deuteron model. We are also indebted to H. Arenhövel and O. Bohigas for enlightening discussions about the sum rules. We also extend our thanks to J. Wu and C. Chang who applied their preequilibrium model to the specific case of our photonuclear experiments on Pb.

We gratefully acknowledge the help of J. Ahrens and U. Kneissl during the first stages of this work. Finally we appreciated very much all the critical comments provided by B. Berman and L. Cardman.

References

1) J. Ahrens *et al.*, Proc. Int. Conf. on nuclear structure studies using electron scattering and photoreaction, Sendai, 1972, p. 213;
J. Ahrens *et al.*, Nucl. Phys. **A251** (1975) 479
2) J.S. Levinger, Phys. Rev. **84** (1951) 43
3) L.W. Jones and K.M. Terwilliger, Phys. Rev. **91** (1953) 699
4) J.M. Wyckoff, Phys. Rev. **159** (1967) 953
5) A. Veyssière, H. Beil, R. Bergère, P. Carlos and A. Leprêtre, Nucl. Phys. **A159** (1970) 561
6) G.G. Jonsson and B. Forkman, Nucl. Phys. **A107** (1968) 52;
K. Lindgren and G.G. Jonsson, Nucl. Phys. **A166** (1971) 643
7) J. Ahrens, H. Borchert, A. Zieger and B. Ziegler, Nucl. Instr. **108** (1973) 517
8) H. A. Gimm and J.H. Hubbel, N.B.S. Technical note 968 (1968);
N.K. Sherman, C.K. Ross and K. H. Lokan, Int. Conf. on Nucl. Phys. with electromagnetic interactions, Mainz, 1979; Contribution paper 4.31
9) T.A. Gabriel and R.G. Alsmiller, Phys. Rev. **182** (1969) 1035;
T.A. Gabriel, Phys. Rev. **C13** (1976) 240
10) J. Arends *et al.*, Proc. Int. Conf. on nuclear physics, Berkeley to be published; and Proc. Workshop on perspectives in electro- and photonuclear physics, Saclay, to be published;
H. Rost, Bonn University report BONN IR-80-10 (1980)
11) B.L. Berman and S.C. Fultz, Rev. Mod. Phys. **47** (1975) 713
12) A. Veyssière, H. Beil, R. Bergère, P. Carlos, J. Fagot, A. Leprêtre and J. Ahrens, Nucl. Instr. **165** (1979) 417
13) H. Beil, R. Bergère and A. Veyssière, Nucl. Instr. **67** (1969) 293
14) A. Leprêtre *et al.*, to be published
15) J.R. Wu and C.C. Chang, Phys. Rev. **C16** (1977) 1812;
J.R. Wu and C.C. Chang, private communication
16) K. Shoda, Phys. Reports **53** (1979) 343
17) T. Saito, S. Oikawa, K. Shoda, M. Sugawara, H. Miyase and A. Suzuki, Phys. Rev. **C16** (1977) 958;
A. Suzuki *et al.*, Nucl. Phys. **A257** (1976) 477
18) H.S. Pruys *et al.*, Nucl. Phys. **A316** (1979) 365
19) R. Bergère, in Nuclear physics with electromagnetic interaction, Mainz 1979, Lecture Notes in Physics **108** (Springer) p. 138
20) J.S. Pringle, A.G. Flowers, D. Brandford, J.C. McGeorge and C.H. Zimmermann, Nucl. Phys. **A325** (1979) 63
21) Nucl. Data Tables **9** (1971) 267; **7** (1970) 565
22) A. Leprêtre *et al.*, Phys. Lett. **79B** (1978) 43
23) B. Ziegler, Proc. Workshop on few body systems and electromagnetic interactions, Frascati (1978), Lecture notes in Physics **86** (Springer) p. 101
24) H. Arenhövel, in Nuclear physics with electromagnetic interactions, Mainz (1979), Lecture notes in Physics **108** (Springer) p. 159
25) S.B. Gerasimov, Phys. Lett. **13** (1964) 240
26) A. Leprêtre *et al.*, Nucl. Phys. **A219** (1974) 39
27) R. Bergère *et al.*, Nucl. Phys. **A121** (1968) 463;
R. Bergère *et al.*, Nucl. Phys. **A133** (1969) 417
28) A. Veyssière *et al.*, Nucl. Phys. **A199** (1973) 45
29) J.T. Caldwell, E.J. Dowdy, B.L. Berman, R.A. Alvarez and P. Meyer, Phys. Rev. **C21** (1980) 1215
30) L.C. Maximon and H.A. Gimm, to be published

31) A. Arima, G.E. Brown, H. Hyuga and M. Ichimura, Nucl. Phys. **A205** (1973) 27
32) W.T. Weng, T.T.S. Kuo and G.E. Brown, Phys. Lett. **46B** (1973) 329
33) M. Gari, H. Hebach, B. Sommer and J.G. Zabolitzky, Phys. Rev. Lett. **41** (1978) 1288
34) D.G. Sandler and J.W. Clark, Nucl. Phys. **A342** (1980) 213
35) G.E. Brown and M. Rho, Nucl. Phys. **A338** (1980) 269
36) J.I. Fujita and M. Hirata, Phys. Lett. **37B** (1971) 237;
J.I. Fujita, S. Yamaji and M. Hirata, J. Phys. Soc. Japan **33** (1972) 541;
J.I. Fujita and M. Ichimura, Mesons in nuclei, ed. M. Rho and D.H. Wilkinson (North-Holland, Amsterdam, 1979) p. 627
37) E. Hadjimichael and G.E. Brown, to be published
38) J.S. Levinger, Phys. Lett. **82B** (1979) 181
39) J.M. Laget, Nucl. Phys. **A312** (1978) 265; and private communication
40) B. Ziegler, in Nuclear physics with electromagnetic interactions, Mainz 1979, Lecture Notes in Physics **108** (Springer) p. 148